Differential modulation of the default mode network via serotonin-1A receptors

Andreas Hahn[a], Wolfgang Wadsak[b], Christian Windischberger[c], Pia Baldinger[a], Anna S. Höflich[a], Jan Losak[a], Lukas Nics[b], Cécile Philippe[b], Georg S. Kranz[a], Christoph Kraus[a], Markus Mitterhauser[b], Georgios Karanikas[b], Siegfried Kasper[a], and Rupert Lanzenberger[a,1]

[a]Department of Psychiatry and Psychotherapy, [b]Department of Nuclear Medicine, and [c]Magnetic Resonance Center of Excellence, Center for Medical Physics and Biomedical Engineering, Medical University of Vienna, 1090 Vienna, Austria

Edited by Marcus E. Raichle, Washington University in St. Louis, St. Louis, MO, and approved January 4, 2012 (received for review October 19, 2011)

Reflecting one's mental self is a fundamental process for evaluating the personal relevance of life events and for moral decision making and future envisioning. Although the corresponding network has been receiving growing attention, the driving neurochemical mechanisms of the default mode network (DMN) remain unknown. Here we combined positron emission tomography and functional magnetic resonance imaging to investigate modulations of the DMN via serotonin-1A receptors (5-HT_{1A}), separated for 5-HT autoinhibition (dorsal raphe nucleus) and local inhibition (heteroreceptors in projection areas). Using two independent approaches, regional 5-HT_{1A} binding consistently predicted DMN activity in the retrosplenial cortex for resting-state functional magnetic resonance imaging and the Tower of London task. On the other hand, both local and autoinhibitory 5-HT_{1A} binding inversely modulated the posterior cingulate cortex, the strongest hub in the resting human brain. In the frontal part of the DMN, a negative association was found between the dorsal medial prefrontal cortex and local 5-HT_{1A} inhibition. Our results indicate a modulation of key areas involved in self-referential processing by serotonergic neurotransmission, whereas variations in 5-HT_{1A} binding explained a considerable amount of the individual variability in the DMN. Moreover, the brain regions associated with distinct introspective functions seem to be specifically regulated by the different 5-HT_{1A} binding sites. Together with previously reported modulations of dopamine and GABA, this regional specialization suggests complex interactions of several neurotransmitters driving the default mode network.

functional connectivity | resting-state networks | neurotransmitter modulation

Without performing particular tasks, the human brain maintains a baseline state (1) that is characterized by the activation of a set of regions known as the default mode network (DMN) (2). This intrinsically organized (3) and individually adaptive (4, 5) network has been implicated in introspective processes including, among others, episodic memory and theory of mind (6, 7). Accordingly, the DMN can be activated by direct confrontation with moral dilemma (8) and self-referential judgments of mental states and personal future (9). The DMN has also been identified in the resting state, which encourages the processing of introspective thoughts or "mind wandering" (10), within both positron emission tomography (PET) (2) as well as spontaneous fluctuations in blood oxygenation level-dependent (BOLD) signal (11). Importantly, the spontaneous BOLD activity acquired at rest shows similar connectivity patterns compared with task-evoked responses and anatomical connections (12–14). On the other hand, the DMN was initially discovered by its consistent deactivation throughout various cognitively demanding tasks (15) and during externally focused attention (1), from which the name "task-negative network" emerged (3). Although this network has been robustly identified across imaging modalities and tasks, there is still considerable variability between subjects (11, 16). For instance, individual DMN activity seems to be associated with task performance (17), learning (4, 5), and creativity (18) as well as personal emotionality (19). Furthermore, DMN coupling increases with maturation (20) and declines again in normal aging (21). Hence, it is hardly surprising that alterations in the functional connectivity networks have been found in almost every mental disorder, including depression (6, 22, 23), anxiety disorders (24), schizophrenia (25), attention deficit hyperactivity disorder (26), and Alzheimer's disease (21, 27). This emphasizes the importance of individual variations in the default mode network across subjects and patient populations.

Despite the growing interest in the DMN and its robust identification with PET and spontaneous BOLD fluctuations, its underlying neurochemical modulators substantially remain unknown. Cerebral blood flow, and hence the BOLD contrast, is locally controlled via glutamate signaling (28) but globally regulated by monoamine neurotransmitters including dopamine (29), noradrenaline (30), and serotonin (5-HT) (31). Within the 5-HT system, several receptor subtypes show considerable spatial overlap with the DMN (32), whereas the main inhibitory receptor (5-HT_{1A}) takes an exceptional role due to its dual expression. Located on cell bodies of serotonergic neurons in the midbrain raphe nuclei, 5-HT_{1A} receptors have an autoinhibitory function on tonic serotonergic neurotransmission and, hence, represent a putative indicator of 5-HT cell firing (33, 34) and serotonin synthesis (35). On the other hand, within projection areas, 5-HT_{1A} heteroreceptors are expressed on glutamate and GABA neurons (36, 37), which in turn drive the hemodynamic response to neural processing (28).

Based on this regulatory cascade of the BOLD signal and their intense spatial overlap (Fig. 1), we expected to find widespread modulations of 5-HT_{1A} receptors onto the DMN. Specifically, this study aimed to evaluate whether both local and autoinhibitory 5-HT_{1A} binding may predict the individual variability in DMN activity. To test this hypothesis, we combined PET and BOLD functional magnetic resonance imaging (fMRI) data obtained from 28 healthy subjects. For a thorough evaluation of 5-HT_{1A} associations across tasks, the DMN was calculated from

Author contributions: W.W., C.W., M.M., G.K., S.K., and R.L. designed research; A.H., W.W., C.W., P.B., A.S.H., J.L., L.N., C.P., C.K., M.M., G.K., S.K., and R.L. performed research; A.H., J.L., L.N., C.P., and G.S.K. analyzed data; and A.H., C.W., P.B., A.S.H., G.S.K., C.K., and R.L. wrote the paper.

Conflict of interest statement: Without any relevance to this work, S.K. declares he has received grant/research support from Eli Lilly, Lundbeck A/S, Bristol-Myers Squibb, Servier, Sepracor, GlaxoSmithKline, and Organon; has served as a consultant or on advisory boards for AstraZeneca, Austrian Science Fund, Bristol-Myers Squibb, GlaxoSmithKline, Eli Lilly, Lundbeck A/S, Pfizer, Organon, Sepracor, Janssen, and Novartis; and has served on speakers' bureaus for AstraZeneca, Eli Lilly, Lundbeck A/S, Servier, Sepracor, and Janssen. R.L. has received travel grants and conference speaker honoraria from AstraZeneca and Lundbeck A/S. M.M. and W.W. have received speaker honoraria from Bayer.

This article is a PNAS Direct Submission.

[1]To whom correspondence should be addressed. E-mail: rupert.lanzenberger@meduniwien.ac.at.

This article contains supporting information online at www.pnas.org/lookup/suppl/doi:10.1073/pnas.1117104109/-/DCSupplemental.

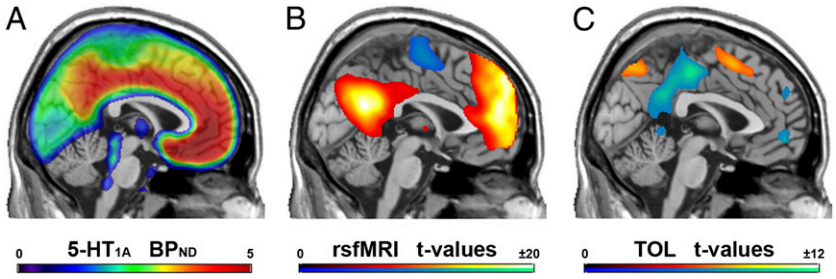

Fig. 1. Average maps across 28 healthy subjects computed for PET and fMRI. (*A*) 5-HT_{1A} receptor BP_{ND} as measured with the radioligand [*carbonyl*-^{11}C]WAY-100635. (*B* and *C*) Independent representations of the DMN ($P < 0.05$, FWE-corrected) were obtained from rsfMRI (*B*) and deactivations within the Tower of London task (*C*). rsfMRI and TOL show inverse patterns because the seed region for rsfMRI was set to the task-negative part of the DMN (3). $x = 0$ mm MNI stereotactic space.

two independent approaches using fMRI, namely (*i*) the spontaneous fluctuations in BOLD signals acquired at rest and (*ii*) the Tower of London (TOL) paradigm, a cognitively demanding task that involves planning and working memory (38).

Results

Resting-State fMRI and 5-HT_{1A} Binding. The default mode network was assessed with functional connectivity analysis from spontaneous BOLD activity at rest. To avoid seed selection bias (39), we computed the DMN from the average fMRI time course of the entire network instead of restricting the seed to a single region. This allows an interpretation beyond simple interregional connectivities but more generally as each voxel's functional contribution to the network.

Similar to previous reports, functional connectivity analysis showed significant involvement in the DMN for the posterior cingulate, retrosplenial, medial prefrontal, and lateral parietal cortices ($P < 0.05$, family-wise error (FWE)-corrected; Fig. 1*B*). In contrast, we found no significant (para)hippocampal contribution (3), which is, however, in line with previous work (16). The task-positive counterpart of the DMN comprised the intraparietal and inferior precentral sulci, inferior precentral gyrus, and supplementary motor area as well as dorsal lateral prefrontal cortex and insula.

5-HT_{1A} receptor binding potentials (BP_{ND}) were estimated with PET and the radioligand [*carbonyl*-^{11}C]WAY-100635. Receptor quantification was carried out for whole-brain maps (Fig. 1*A*) and the dorsal raphe nucleus, which reflect 5-HT_{1A} inhibition via local (i.e., heteroreceptor) and autoreceptor binding, respectively. Hence, entering both variables into a linear regression model enables a separation of local and autoinhibitory 5-HT_{1A} effects as independent predictors of the DMN (i.e., adjusting for regional receptor binding when interpreting 5-HT_{1A} autoinhibition, and vice versa).

For 5-HT_{1A} heteroreceptors, local positive and negative modulations of the DMN were found in the retrosplenial cortex (RSC; $R^2 = 0.64$, $P < 0.05$, FWE-corrected; Fig. 2*A*) and the dorsal medial prefrontal cortex (dmPFC; $R^2 = 0.45$, $P < 0.001$), respectively (Table S1). On the other hand, both 5-HT_{1A} auto- and heteroreceptor binding predicted individual DMN contributions in the posterior cingulate cortex (PCC) but in opposite

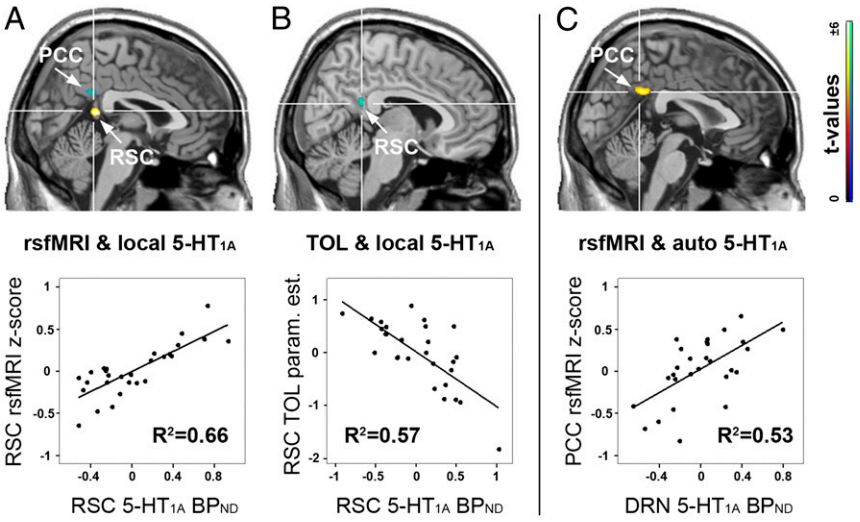

Fig. 2. Modulation of the DMN via 5-HT_{1A} BP_{ND} separated for auto- and heteroreceptors [i.e., dorsal raphe nucleus (DRN) and local 5-HT_{1A} binding sites, respectively]. (*A*) Local 5-HT_{1A} receptors influence individual contributions to the DMN in the RSC. (*B*) Similar to resting-state fMRI (*z* scores in *A*), RSC deactivations (parameter estimates) during the TOL paradigm are modulated by local 5-HT_{1A} binding. The RSC effects in *A* and *B* show inverse patterns due to choice of rsfMRI seed region (Fig. 1 *B* and *C*). (*C*) On the other hand, the PCC is regulated through both 5-HT_{1A} local and autoinhibition in an inverse manner (*A* and *C*), suggesting a well-balanced interaction between dorsal raphe nucleus autoreceptors (*C*) and local 5-HT_{1A} in the PCC expressed on downstream glutamate and GABA neurons (*A*). Images are shown at $P < 0.001$, cluster-level $k = 15$ voxels = 120 mm^3. Scatter plots illustrate the association for the entire cluster. Note that variables are mean-centered after adjustment for nuisance covariates (including correction for regional 5-HT_{1A} binding when interpreting 5-HT_{1A} autoinhibition, and vice versa), which introduces negative values in the plots (see Table S2 for actual BP_{ND} values). $x = 2$, 7, and 3 mm MNI stereotactic space for *A*, *B*, and *C*, respectively.

directions ($R^2 = 0.55$, $P < 0.05$, FWE-corrected and $R^2 = 0.44$, $P < 0.001$, respectively; Fig. 2 *A* and *C* and Table S1). In the task-positive part, a significant association between local 5-HT_{1A} BP_{ND} and the DMN was found in the insula ($R^2 = 0.48$, $P < 0.05$, FWE-corrected; Table S1).

Tower of London fMRI and 5-HT_{1A} Binding. In a second approach, we aimed to validate these findings with an independent representation of the DMN. Because this network exhibits a main characteristic of deactivation during cognitively demanding tasks (3, 15), participants additionally completed the Tower of London paradigm within the same fMRI session (38, 40).

Group analysis showed deactivations predominantly in the posterior DMN and to a lesser extent in medial prefrontal areas and the insula ($P < 0.05$, FWE-corrected; Fig. 1*C*). Task-specific activations were found in inferior and superior parietal areas, precentral gyrus, supplementary motor area, dorsal lateral prefrontal cortex, and anterior insula (Fig. 1*C* and Fig. S1*A*). Compared with resting-state fMRI, the activation pattern obtained from TOL shows great overlap with the DMN task-positive part but exhibits considerably less pronounced deactivations, especially in the mPFC and precuneus (Fig. 1 *B* and *C*).

To assess the influence of 5-HT_{1A} receptors, the individual activation maps from TOL served as dependent variables of the linear regression model. Similar to resting-state analysis, local 5-HT_{1A} binding predicted task-induced deactivations in the RSC ($R^2 = 0.55$, $P < 0.05$, FWE-corrected; Fig. 2*B* and Table S1). In the task-positive counterpart of the DMN, local 5-HT_{1A} effects were present in the precentral gyrus bilaterally ($R^2 = 0.5$, $P < 0.001$; Fig. S1 *B* and *C* and Table S1).

See *SI Results* for evaluation of potential confounders.

Discussion

This work demonstrates considerable modulatory effects of serotonin-1A receptor binding on the default mode network. Specifically, both 5-HT_{1A} auto- and heteroreceptors appear to regulate the posterior part of the midline core system (PCC), engaged when assessing the personal significance of events (9). In contrast, only local 5-HT_{1A} inhibition influences DMN subparts involved in memory-based future envisioning (RSC) (41) and self-referential judgments (dmPFC) (7), but in an inverse manner. Hence, it seems that the different brain areas, which entail various functional aspects of self-referential processing, experience markedly distinct regulations via different 5-HT_{1A} binding sites. This regional specificity via neurotransmitter modulations complements previous work showing that the DMN can be further segregated by taking into account the functional specialization of different brain regions (9, 42–44).

Serotonin-1A Modulations During Rest and Cognitive Tasks. Using two independent approaches, we demonstrate a robust influence of the 5-HT_{1A} receptor on the DMN's retrosplenial cortex. The RSC has been extensively implicated in the processing of episodic memory (44) and future imagination (45). More precisely, it has been suggested to act as a relay station between allocentric and egocentric viewpoints, translating memories and events (indexed by the hippocampus and thalamus) into a personal context (41). With regard to the 5-HT system, episodic memory processing and the RSC experience a considerable influence by tryptophan depletion (46, 47) and the administration of selective serotonin reuptake inhibitors (SSRIs) (48), respectively. Hence, the current study further specifies the modulation of this introspective function by serotonergic neurotransmission to the 5-HT_{1A} receptor subtype.

Comparing the resting state and the TOL task, consistent 5-HT_{1A} effects were only found in the RSC. On the other hand, additional associations were present in different subparts of the DMN for each of the paradigms. Again, although the basic anatomy of the default mode network is similar across tasks (rest, self-referential, and cognitive) and stimulus domains, there is still a functional specialization for each of these (8, 49, 50). Hence, the additional task-related neuroreceptor modulations found in cognitively demanding paradigms may emerge at the cost of missing associations in task-negative parts of the DMN. Such a functional specialization may similarly apply to emotional tasks. For instance, in response to threat-related stimuli, a significant influence of the serotonin-2A receptor (51) and transporter polymorphism (52) on amygdala–prefrontal coupling has been described. These findings demonstrate the relevance of evaluating modulatory effects of different neurotransmitters also in specific paradigms of self-referential and emotional processing.

Posterior Cingulate Cortex. In addition to memory-coding regions (hippocampus, thalamus), the RSC receives intensive input from the PCC (41), which is in turn innervated by the midbrain raphe nuclei (53). Accordingly, we found a modulation of dorsal raphe nucleus 5-HT_{1A} autoreceptor binding onto the PCC and to a lesser extent by local 5-HT_{1A} heteroreceptors. Importantly, this region has been identified as the strongest hub in the resting human brain, with the highest number of functional connections (54). In line with previous reports and similar to the RSC, PCC activity is influenced by tryptophan depletion (55) and SSRI administration (56). Again, these findings indicate that a substantial part of the serotonergic influence on this DMN core region (9) is mediated by the different 5-HT_{1A} binding sites. The negative DMN association in the PCC with local 5-HT_{1A} receptors is, however, not contradictive to the positive modulation via autoreceptors (Fig. 2 *A* and *C*). 5-HT_{1A} autoreceptors attenuate raphe nuclei cell firing (33, 34), leading to reduced 5-HT release at projection sites (35). This decreases local 5-HT_{1A} inhibition of downstream glutamate neurons, which in turn increases BOLD signal (28). Hence, our results suggest a regulation of the DMN's major hub (54) through a well-balanced interaction between 5-HT_{1A} auto- and heteroreceptors. The importance of such a relation between different receptors has been shown in anxiety disorders for this subtype (57) and for the balance between 5-HT_{1A} and 5-HT_{2A} receptors (58) as well as in healthy subjects for 5-HT_{1A} and the serotonin transporter (59).

Medial Prefrontal Cortex and Serotonin-1A in Depression. The associations found here could provide important implications for major depressive disorder (MDD), considering alterations in both 5-HT_{1A} levels (60–62) and DMN function (6, 22, 23). Specifically, the negativity bias in MDD patients has been suggested to emerge from a lack of DMN inhibition in the ventral and dorsal mPFC (63), responsible for coding and reappraisal of self-related stimuli, respectively (49). Moreover, SSRI administration attenuates negative introspective processing of the mPFC in subjects at risk for depression (64). Integrating the negative dmPFC modulation found here leads us to speculate that the deficient inhibition of the DMN in depression could be mediated via the 5-HT_{1A} receptor subtype.

Regional Specificity of Neuroreceptor Modulations. In contrast to our hypothesis of widespread interactions between the DMN via 5-HT_{1A} receptors, the observed effects were regionally specific to certain subparts of the network. This is, however, consistent with previous findings of local DMN modulations by other neurotransmitters. For instance, associations with the DMN have also been found for dopamine and one of its degradation enzymes, the catechol-*O*-methyltransferase (COMT). Here, the COMT val^{158}met polymorphism has been associated with differences in mPFC–PCC connectivity at rest (65) and PCC deactivations during two cognitively demanding paradigms (66). Furthermore, task-related deactivations in ventral mPFC and precuneus are

modulated by a dopamine D1/D2 receptor agonist (67) and striatal dopamine transporter binding (68), respectively. Finally, a significant relation has been reported for GABA concentrations in the anterior cingulate cortex and the local BOLD response in emotional processing (69). Together, these results point toward complex and regionally specific neurotransmitter interactions driving brain networks at rest as well as during cognitive and emotional processing.

Conclusions

To summarize, our results indicate that individual variations in the execution of essential introspective functions experience a considerable regulation by the major inhibitory serotonin receptor. Importantly, local and autoinhibitory 5-HT_{1A} effects exhibited a rather differential influence on areas with distinct functionality. The regional specificity of our findings further suggests that the DMN as a whole and hence the various aspects of self-referential processing are driven by complex distribution patterns of neuronal receptors, including their expression sites on downstream glutamate and GABA neurons.

Materials and Methods

Subjects. Twenty-eight healthy subjects participated in this study (mean age ± SD = 26.5 ± 6.8 y, 17 female), who in part also served as control subjects in previous studies (57, 70–73) (*SI Materials and Methods*). This project was approved by the Ethics Committee of the Medical University of Vienna and the General Hospital of Vienna.

Positron Emission Tomography. PET measurements were carried out at the Department of Nuclear Medicine, Medical University of Vienna, and are essentially described elsewhere (57, 71) (*SI Materials and Methods*). Radiochemical variables for [*carbonyl*-^{11}C]WAY-100635 at the time of injection were injected dose = 381 ± 31.9 MBq, specific activity = 183.2 ± 147.1 MBq/nmol, and mass of unlabeled compound = 3 ± 4.4 μg (mean ± SD); for synthesis, see Wadsak et al. (74).

Serotonin-1A (5-HT_{1A}) autoreceptor binding of the dorsal raphe nucleus was obtained as described previously (57). A spherical region of interest of 4-mm diameter was defined manually within two slices of the original summed PET image (57, 71, 75, 76). This yields a representative estimate of autoreceptor binding because in the human raphe nuclei, the majority (80–100%) of 5-HT_{1A} receptors is expressed on cell bodies of serotonergic neurons (77). PET scans were then motion-corrected and normalized to Montreal Neurological Institute (MNI) space using SPM8 (Wellcome Trust Centre for Neuroimaging; http://www.fil.ion.ucl.ac.uk/spm) via the corresponding T1-weighted MRI (*SI Materials and Methods*). To assess local inhibitory effects, whole-brain 5-HT_{1A} maps were computed from the final normalized and resliced images comprising a voxel size of 2 × 2 × 2 mm.

Quantification of the 5-HT_{1A} receptor binding potential (78) was done in PMOD 3.3 (PMOD Technologies) with an improved version (79) of the noninvasive Logan plot (80) for both the dorsal raphe nucleus region of interest and voxel-wise 5-HT_{1A} maps. The model includes two major advantages, namely no assumption of compartmental model configuration (80) and stable results in the presence of noise (79), which makes it particularly suitable for voxel-wise applications. The cerebellar gray matter (excluding vermis) served as a reference region due to negligible specific receptor binding (81). The time from which the Logan plot describes a straight line (t^*) was automatically estimated from the insula with PMOD 3.3 and was 19.6 ± 4.5 min. 5-HT_{1A} receptor binding potentials are shown in Fig. 1*A* and Table S2.

Functional Magnetic Resonance Imaging. In addition to PET, each subject underwent MRI measurements in a 3-T Medspec S300 (Bruker Biospin) while performing a resting-state scan and the TOL paradigm. The two paradigms lasted for 360 and 470 s, respectively, and were acquired with the same scanning parameters as described previously (40, 73, 82) (*SI Materials and Methods*).

Standard preprocessing for both paradigms was carried out in SPM8 using default parameters if not specified differently. This included correction for slice-timing differences and head motion (quality = 1), normalization to MNI space (affine regularization = average-sized template), and spatial smoothing with a Gaussian kernel of 9 mm.

Resting-State Functional Connectivity Analysis. Resting-state fMRI (rsfMRI) data were further processed in MATLAB R2010a (MathWorks) according to an optimized procedure (82). Potential confounders of ventricular, white matter, and global signal as well as motion parameters were corrected for using linear regression analysis, and a band-pass filter was applied (12-term finite impulse response (FIR) filter, 0.007 < f < 0.08 Hz). To avoid seed selection bias (39), functional connectivity analysis of the DMN was computed in several steps. First, a seed region (83) was defined within the posterior cingulate cortex (cubic volume of 3 × 3 × 3 voxels = 216 mm^3 centered at *x*/*y*/*z* = 0/−52/30 mm), because this represents the main functional connectivity hub of the human brain (54). The averaged BOLD signal time course was then cross-correlated voxel-wise with the entire brain, and correlation maps were converted to *z* values by Fisher's *r*-to-*z* transformation. A binary map of the DMN was obtained by applying a one-sample *t* test across subjects and thresholding at $P < 0.05$, FWE-corrected for multiple comparisons at the voxel level. Similarly, a second DMN mask was created from a seed within the mPFC [*x*/*y*/*z* = 0/50/22 mm (54)], which represents the frontal part of the DMN core network (9). The final seed region was then calculated as the intersection of the two binary DMN masks, covering a volume of 44.8 cm^3 (=5,604 voxels). Hence, the obtained seed is not restricted to a particular region, but comprises a conjunction of several network nodes (84). Again, cross-correlation was then computed between the seed's averaged BOLD signal time course and the brain, followed by *z* transformation. This approach enables an interpretation of the resulting *z* values not simply as connectivity between two regions but more generally as how strong each voxel is functionally involved in the network (i.e., each voxel's functional connectivity with the network mean).

Tower of London Task. The TOL paradigm is a cognitively demanding task that requires planning, spatial working memory, and problem solving (38, 40) (*SI Materials and Methods*). Following previous associations between TOL and the dopamine system (67), this paradigm provides a reasonable choice for assessing neurotransmitter modulations of the DMN.

For first-level data analysis, the boxcar function obtained from the design was convolved with a standard hemodynamic response function in SPM8. Similar to the resting state, additional nuisance regressors from realignment parameters and ventricular and white matter signals were included in the model. Notably, the activations obtained from the TOL task exhibit the inverse pattern compared with resting-state analysis (Fig. 1 *B* and *C*), because the seed region of the rsfMRI connectivity calculations was set to the task-negative part of the DMN (3).

Statistical Analysis. To investigate both local and autoinhibitory effects of 5-HT_{1A} binding on the DMN, a linear regression analysis was carried out using the biological parametric mapping (BPM) toolbox (85) for SPM8. The toolbox enables the calculation of voxel-by-voxel and region of interest-by-voxel associations within the same model. Hence, independent variables were defined as 5-HT_{1A} BP_{ND} whole-brain maps and dorsal raphe nucleus receptor binding, representing local inhibition and autoinhibition via 5-HT_{1A}, respectively. On the other hand, rsfMRI *z* maps reflecting the DMN were used as dependent variables. The influence of 5-HT_{1A} binding on de-/activations during the TOL paradigm were evaluated in the same fashion, that is, using fMRI maps with parameter estimates as dependent variables.

Because 5-HT_{1A} BP_{ND} of the dorsal raphe nucleus is highly correlated with postsynaptic receptor binding (57, 86–88), we aimed to disentangle local from autoinhibitory effects. Using the BPM toolbox, this was realized by adjusting for regional 5-HT_{1A} binding when interpreting 5-HT_{1A} autoinhibition, and vice versa. This enables an evaluation of the two variables as independent predictors of the DMN (i.e., assuming the same local 5-HT_{1A} binding across subjects for the assessment of autoinhibition, and vice versa). Additional nuisance covariates included age for rsfMRI analysis as well as age and reaction times for the TOL paradigm.

All calculations were spatially restricted to areas with a robust representation of the DMN and fMRI de-/activations, respectively. This was assessed by one-sample *t* tests for each fMRI paradigm ($P < 0.05$, FWE-corrected at voxel level; Fig. 1) with a separate evaluation of task-positive and -negative networks (Table S1). To provide a thorough assessment, we report results at an uncorrected threshold of $P < 0.001$ voxel level with a minimum cluster size of 120 mm^3 (k = 15 voxels). However, considering the spatial constraints (339 and 192 cm^3 for resting state and TOL, respectively), correction for multiple comparisons was applied at $P < 0.05$, FWE-corrected for peak voxels or cluster extent (the latter at $P < 0.001$, uncorrected voxel level). All statistical tests were carried out two-tailed.

To illustrate the association between 5-HT_{1A} binding and the DMN, scatter plots were created in MATLAB R2010a. However, simply plotting the dependent variable (Y) against the target explanatory (independent) variable

(X) does not take into account the remaining independent variables (Z, nuisance covariates), which are still included in the regression model. Hence, partial regression plots were used to adjust the scatter plot for variables of noninterest (89, 90). This is achieved by plotting the residuals of the regression of Y on the remaining independent variables Z against the residuals of the regression of X on the remaining independent variables Z. Notably, this adjustment implies that plotted values can take positive and negative values because residuals are mean-centered (i.e., mean = 0).

ACKNOWLEDGMENTS. We thank the medical and technical teams of the Department of Psychiatry and Psychotherapy (P. Stein, M. Fink, C. Spindelegger, U. Moser, E. Akimova, and M. Savli), the PET Center at the Department of Nuclear Medicine (K. Kletter, R. Dudczak, L.-K. Mien, T. Zenz, and A. Krcal), and the Magnetic Resonance Centre of Excellence (E. Moser and F. Gerstl). This research was funded by Austrian National Bank Grant P11468 and Austrian Science Fund Grant P 23021 (to R.L.). A.H. is a recipient of a DOC fellowship of the Austrian Academy of Sciences at the Department of Psychiatry and Psychotherapy.

1. Gusnard DA, Raichle ME, Raichle ME (2001) Searching for a baseline: Functional imaging and the resting human brain. *Nat Rev Neurosci* 2:685–694.
2. Raichle ME, et al. (2001) A default mode of brain function. *Proc Natl Acad Sci USA* 98: 676–682.
3. Fox MD, et al. (2005) The human brain is intrinsically organized into dynamic, anticorrelated functional networks. *Proc Natl Acad Sci USA* 102:9673–9678.
4. Sun FT, Miller LM, Rao AA, D'Esposito M (2007) Functional connectivity of cortical networks involved in bimanual motor sequence learning. *Cereb Cortex* 17:1227–1234.
5. Lewis CM, Baldassarre A, Committeri G, Romani GL, Corbetta M (2009) Learning sculpts the spontaneous activity of the resting human brain. *Proc Natl Acad Sci USA* 106:17558–17563.
6. Broyd SJ, et al. (2009) Default-mode brain dysfunction in mental disorders: A systematic review. *Neurosci Biobehav Rev* 33:279–296.
7. Buckner RL, Andrews-Hanna JR, Schacter DL (2008) The brain's default network: Anatomy, function, and relevance to disease. *Ann N Y Acad Sci* 1124:1–38.
8. Harrison BJ, et al. (2008) Consistency and functional specialization in the default mode brain network. *Proc Natl Acad Sci USA* 105:9781–9786.
9. Andrews-Hanna JR, Reidler JS, Sepulcre J, Poulin R, Buckner RL (2010) Functional-anatomic fractionation of the brain's default network. *Neuron* 65:550–562.
10. Mason MF, et al. (2007) Wandering minds: The default network and stimulus-independent thought. *Science* 315:393–395.
11. Biswal BB, et al. (2010) Toward discovery science of human brain function. *Proc Natl Acad Sci USA* 107:4734–4739.
12. Vincent JL, et al. (2007) Intrinsic functional architecture in the anaesthetized monkey brain. *Nature* 447(7140):83–86.
13. Greicius MD, Supekar K, Menon V, Dougherty RF (2009) Resting-state functional connectivity reflects structural connectivity in the default mode network. *Cereb Cortex* 19(1):72–78.
14. Damoiseaux JS, Greicius MD (2009) Greater than the sum of its parts: A review of studies combining structural connectivity and resting-state functional connectivity. *Brain Struct Funct* 213:525–533.
15. Shulman GL, et al. (1997) Searching for activations that generalize over tasks. *Hum Brain Mapp* 5:317–322.
16. Damoiseaux JS, et al. (2006) Consistent resting-state networks across healthy subjects. *Proc Natl Acad Sci USA* 103:13848–13853.
17. Hampson M, Driesen NR, Skudlarski P, Gore JC, Constable RT (2006) Brain connectivity related to working memory performance. *J Neurosci* 26:13338–13343.
18. Takeuchi H, et al. (2011) Failing to deactivate: The association between brain activity during a working memory task and creativity. *Neuroimage* 55:681–687.
19. Volkow ND, et al. (2011) Positive emotionality is associated with baseline metabolism in orbitofrontal cortex and in regions of the default network. *Mol Psychiatry* 16: 818–825.
20. Fair DA, et al. (2008) The maturing architecture of the brain's default network. *Proc Natl Acad Sci USA* 105:4028–4032.
21. Lustig C, et al. (2003) Functional deactivations: Change with age and dementia of the Alzheimer type. *Proc Natl Acad Sci USA* 100:14504–14509.
22. Anand A, et al. (2005) Activity and connectivity of brain mood regulating circuit in depression: A functional magnetic resonance study. *Biol Psychiatry* 57:1079–1088.
23. Sheline YI, et al. (2009) The default mode network and self-referential processes in depression. *Proc Natl Acad Sci USA* 106:1942–1947.
24. Liao W, et al. (2010) Selective aberrant functional connectivity of resting state networks in social anxiety disorder. *Neuroimage* 52:1549–1558.
25. Salvador R, et al. (2010) Overall brain connectivity maps show cortico-subcortical abnormalities in schizophrenia. *Hum Brain Mapp* 31:2003–2014.
26. Castellanos FX, et al. (2008) Cingulate-precuneus interactions: A new locus of dysfunction in adult attention-deficit/hyperactivity disorder. *Biol Psychiatry* 63:332–337.
27. Greicius MD, Srivastava G, Reiss AL, Menon V (2004) Default-mode network activity distinguishes Alzheimer's disease from healthy aging: Evidence from functional MRI. *Proc Natl Acad Sci USA* 101:4637–4642.
28. Attwell D, Iadecola C (2002) The neural basis of functional brain imaging signals. *Trends Neurosci* 25:621–625.
29. Krimer LS, Muly, EC, III, Williams GV, Goldman-Rakic PS (1998) Dopaminergic regulation of cerebral cortical microcirculation. *Nat Neurosci* 1:286–289.
30. Raichle ME, Hartman BK, Eichling JO, Sharpe LG (1975) Central noradrenergic regulation of cerebral blood flow and vascular permeability. *Proc Natl Acad Sci USA* 72: 3726–3730.
31. Cohen Z, Bonvento G, Lacombe P, Hamel E (1996) Serotonin in the regulation of brain microcirculation. *Prog Neurobiol* 50:335–362.
32. Saulin A, Savli M, Lanzenberger R (September 24, 2011) Serotonin and molecular neuroimaging in humans using PET. *Amino Acids*, 10.1007/s00726-011-1078-9.
33. Hillegaart V, Hjorth S, Ahlenius S (1990) Effects of 5-HT and 8-OH-DPAT on forebrain monoamine synthesis after local application into the median and dorsal raphe nuclei of the rat. *J Neural Transm* 81(2):131–145.
34. Bonvento G, Lacombe P, Seylaz J (1989) Effects of electrical stimulation of the dorsal raphe nucleus on local cerebral blood flow in the rat. *J Cereb Blood Flow Metab* 9: 251–255.
35. Evans AK, et al. (2008) Evidence for serotonin synthesis-dependent regulation of in vitro neuronal firing rates in the midbrain raphe complex. *Eur J Pharmacol* 590(1–3):136–149.
36. Fink KB, Göthert M (2007) 5-HT receptor regulation of neurotransmitter release. *Pharmacol Rev* 59:360–417.
37. Mengod G, Cortés R, Vilaró MT, Hoyer D (2010) Distribution of 5-HT receptors in the central nervous system. *Handbook of the Behavioral Neurobiology of Serotonin*, eds Müller CP, Jacobs BL (Academic, London).
38. Baker SC, et al. (1996) Neural systems engaged by planning: A PET study of the Tower of London task. *Neuropsychologia* 34:515–526.
39. Cole DM, Smith SM, Beckmann CF (2010) Advances and pitfalls in the analysis and interpretation of resting-state FMRI data. *Front Syst Neurosci* 4:8.
40. Schöpf V, et al. (2011) Model-free fMRI group analysis using FENICA. *Neuroimage* 55 (1):185–193.
41. Vann SD, Aggleton JP, Maguire EA (2009) What does the retrosplenial cortex do? *Nat Rev Neurosci* 10:792–802.
42. Sestieri C, Corbetta M, Romani GL, Shulman GL (2011) Episodic memory retrieval, parietal cortex, and the default mode network: Functional and topographic analyses. *J Neurosci* 31:4407–4420.
43. Stawarczyk D, Majerus S, Maquet P, D'Argembeau A (2011) Neural correlates of ongoing conscious experience: Both task-unrelatedness and stimulus-independence are related to default network activity. *PLoS One* 6:e16997.
44. Dastjerdi M, et al. (2011) Differential electrophysiological response during rest, self-referential, and non-self-referential tasks in human posteromedial cortex. *Proc Natl Acad Sci USA* 108:3023–3028.
45. Botzung A, Denkova E, Manning L (2008) Experiencing past and future personal events: Functional neuroimaging evidence on the neural bases of mental time travel. *Brain Cogn* 66:202–212.
46. van der Veen FM, et al. (2006) Acute tryptophan depletion reduces activation in the right hippocampus during encoding in an episodic memory task. *Neuroimage* 31: 1188–1196.
47. Mendelsohn D, Riedel WJ, Sambeth A (2009) Effects of acute tryptophan depletion on memory, attention and executive functions: A systematic review. *Neurosci Biobehav Rev* 33:926–952.
48. Schwarz AJ, Gozzi A, Reese T, Bifone A (2007) In vivo mapping of functional connectivity in neurotransmitter systems using pharmacological MRI. *Neuroimage* 34: 1627–1636.
49. Northoff G, et al. (2006) Self-referential processing in our brain—A meta-analysis of imaging studies on the self. *Neuroimage* 31:440–457.
50. Laird AR, et al. (2009) Investigating the functional heterogeneity of the default mode network using coordinate-based meta-analytic modeling. *J Neurosci* 29:14496–14505.
51. Fisher PM, et al. (2009) Medial prefrontal cortex 5-HT(2A) density is correlated with amygdala reactivity, response habituation, and functional coupling. *Cereb Cortex* 19: 2499–2507.
52. Pezawas L, et al. (2005) 5-HTTLPR polymorphism impacts human cingulate-amygdala interactions: A genetic susceptibility mechanism for depression. *Nat Neurosci* 8: 828–834.
53. Michelsen KA, Schmitz C, Steinbusch HWM (2007) The dorsal raphe nucleus—From silver stainings to a role in depression. *Brain Res Brain Res Rev* 55:329–342.
54. Tomasi D, Volkow ND (2011) Functional connectivity hubs in the human brain. *Neuroimage* 57:908–917.
55. Kunisato Y, et al. (2011) Modulation of default-mode network activity by acute tryptophan depletion is associated with mood change: A resting state functional magnetic resonance imaging study. *Neurosci Res* 69(2):129–134.
56. Matthews SC, et al. (2010) Escitalopram attenuates posterior cingulate activity during self-evaluation in healthy volunteers. *Psychiatry Res* 182(2):81–87.
57. Hahn A, et al. (2010) Escitalopram enhances the association of serotonin-1A autoreceptors to heteroreceptors in anxiety disorders. *J Neurosci* 30:14482–14489.
58. Michelsen KA, Prickaerts J, Steinbusch HW (2008) The dorsal raphe nucleus and serotonin: Implications for neuroplasticity linked to major depression and Alzheimer's disease. *Prog Brain Res* 172:233–264.
59. Bose SK, et al. (2011) Presynaptic 5-HT1A is related to 5-HTT receptor density in the human brain. *Neuropsychopharmacology* 36:2258–2265.
60. Drevets WC, et al. (2000) Serotonin type-1A receptor imaging in depression. *Nucl Med Biol* 27:499–507.
61. Parsey RV, et al. (2010) Higher serotonin 1A binding in a second major depression cohort: Modeling and reference region considerations. *Biol Psychiatry* 68(2):170–178.
62. Hirvonen J, et al. (2008) Decreased brain serotonin 5-HT1A receptor availability in medication-naive patients with major depressive disorder: An in-vivo imaging study using PET and [carbonyl-^{11}C]WAY-100635. *Int J Neuropsychopharmacol* 11:465–476.

63. Lemogne C, Delaveau P, Freton M, Guionnet S, Fossati P (2012) Medial prefrontal cortex and the self in major depression. *J Affect Disord* 136(1-2):e1–e11.
64. Di Simplicio M, Norbury R, Harmer CJ (March 1, 2011) Short-term antidepressant administration reduces negative self-referential processing in the medial prefrontal cortex in subjects at risk for depression. *Mol Psychiatry,* 10.1038/mp.2011.16.
65. Liu B, et al. (2010) Prefrontal-related functional connectivities within the default network are modulated by COMT val^{158}met in healthy young adults. *J Neurosci* 30(1): 64–69.
66. Stokes PR, Rhodes RA, Grasby PM, Mehta MA (2011) The effects of the COMT val$^{108/158}$met polymorphism on BOLD activation during working memory, planning, and response inhibition: A role for the posterior cingulate cortex? *Neuropsychopharmacology* 36:763–771.
67. Nagano-Saito A, Liu J, Doyon J, Dagher A (2009) Dopamine modulates default mode network deactivation in elderly individuals during the Tower of London task. *Neurosci Lett* 458(1):1–5.
68. Tomasi D, et al. (2009) Dopamine transporters in striatum correlate with deactivation in the default mode network during visuospatial attention. *PLoS One* 4:e6102.
69. Northoff G, et al. (2007) GABA concentrations in the human anterior cingulate cortex predict negative BOLD responses in fMRI. *Nat Neurosci* 10:1515–1517.
70. Stein P, et al. (2008) The serotonin-1A receptor distribution in healthy men and women measured by PET and [carbonyl-^{11}C]WAY-100635. *Eur J Nucl Med Mol Imaging* 35:2159–2168.
71. Lanzenberger RR, et al. (2007) Reduced serotonin-1A receptor binding in social anxiety disorder. *Biol Psychiatry* 61:1081–1089.
72. Fink M, et al. (2009) Lateralization of the serotonin-1A receptor distribution in language areas revealed by PET. *Neuroimage* 45:598–605.
73. Hahn A, et al. (2011) Reduced resting-state functional connectivity between amygdala and orbitofrontal cortex in social anxiety disorder. *Neuroimage* 56:881–889.
74. Wadsak W, et al. (2007) Simple and fully automated preparation of [carbonyl-^{11}C] WAY-100635. *Radiochimica Acta* 95:417–422.
75. Spindelegger C, et al. (2009) Influence of escitalopram treatment on 5-HT 1A receptor binding in limbic regions in patients with anxiety disorders. *Mol Psychiatry* 14: 1040–1050.
76. Sullivan GM, et al. (2009) Positron emission tomography quantification of serotonin-1A receptor binding in medication-free bipolar depression. *Biol Psychiatry* 66: 223–230.
77. Hornung JP (2010) The neuroanatomy of the serotonergic system. *Handbook of the Behavioral Neurobiology of Serotonin*, eds Müller CP, Jacobs BL (Academic, London).
78. Innis RB, et al. (2007) Consensus nomenclature for in vivo imaging of reversibly binding radioligands. *J Cereb Blood Flow Metab* 27:1533–1539.
79. Varga J, Szabo Z (2002) Modified regression model for the Logan plot. *J Cereb Blood Flow Metab* 22:240–244.
80. Logan J, et al. (1996) Distribution volume ratios without blood sampling from graphical analysis of PET data. *J Cereb Blood Flow Metab* 16:834–840.
81. Hall H, et al. (1997) Autoradiographic localization of 5-HT1A receptors in the post-mortem human brain using [^{3}H]WAY-100635 and [^{11}C]WAY-100635. *Brain Res* 745 (1-2):96–108.
82. Weissenbacher A, et al. (2009) Correlations and anticorrelations in resting-state functional connectivity MRI: A quantitative comparison of preprocessing strategies. *Neuroimage* 47:1408–1416.
83. Biswal B, Yetkin FZ, Haughton VM, Hyde JS (1995) Functional connectivity in the motor cortex of resting human brain using echo-planar MRI. *Magn Reson Med* 34: 537–541.
84. Vaishnavi SN, et al. (2010) Regional aerobic glycolysis in the human brain. *Proc Natl Acad Sci USA* 107:17757–17762.
85. Casanova R, et al. (2007) Biological parametric mapping: A statistical toolbox for multimodality brain image analysis. *Neuroimage* 34:137–143.
86. Rabiner EA, et al. (2002) A database of [(11)C]WAY-100635 binding to 5-HT(1A) receptors in normal male volunteers: Normative data and relationship to methodological, demographic, physiological, and behavioral variables. *Neuroimage* 15: 620–632.
87. Borg J, Andrée B, Lundberg J, Halldin C, Farde L (2006) Search for correlations between serotonin 5-HT1A receptor expression and cognitive functions—A strategy in translational psychopharmacology. *Psychopharmacology (Berl)* 185:389–394.
88. Drevets WC, et al. (2007) Serotonin-1A receptor imaging in recurrent depression: Replication and literature review. *Nucl Med Biol* 34:865–877.
89. Velleman P, Welsch R (1981) Efficient computing of regression diagnostics. *Am Stat* 35:234–242.
90. Moya-Laraño J, Corcobado G (2008) Plotting partial correlation and regression in ecological studies. *Web Ecol* 8:35–46.